AAAS
Ultrafast Science
Volume 2022, Article ID 9754919, 10 pages
https://doi.org/10.34133/2022/9754919

Ultrafast Science
A SCIENCE PARTNER JOURNAL

Research Article

Factor 30 Pulse Compression by Hybrid Multipass Multiplate Spectral Broadening

Marcus Seidel,[1] **Prannay Balla**,[1,2,3] **Chen Li**,[1] **Gunnar Arisholm**,[4] **Lutz Winkelmann**,[1] **Ingmar Hartl**,[1] **and Christoph M. Heyl**[1,2,3]

[1]*Deutsches Elektronen-Synchrotron DESY, Notkestrasse 85, 22607 Hamburg, Germany*
[2]*Helmholtz Institute Jena, Fröbelstieg 3, 07743 Jena, Germany*
[3]*GSI Helmholtzzentrum für Schwerionenforschung GmbH, Planckstrasse 1, 64291 Darmstadt, Germany*
[4]*FFI (Norwegian Defence Research Establishment), P.O. Box 25, NO-2027 Kjeller, Norway*

Correspondence should be addressed to Marcus Seidel; marcus.seidel@desy.de

Received 23 October 2021; Accepted 15 February 2022; Published 1 April 2022

As ultrafast laser technology advances towards ever higher peak and average powers, generating sub-50 fs pulses from laser architectures that exhibit best power-scaling capabilities remains a major challenge. Here, we present a very compact and highly robust method to compress 1.24 ps pulses to 39 fs by means of only a single spectral broadening stage which neither requires vacuum parts nor custom-made optics. Our approach is based on the hybridization of the multiplate continuum and the multipass cell spectral broadening techniques. Their combination leads to significantly higher spectral broadening factors in bulk material than what has been reported from either method alone. Moreover, our approach efficiently suppresses adverse features of single-pass bulk spectral broadening. We use a burst-mode Yb:YAG laser emitting pulses with 80 MW peak power that are enhanced to more than 1 GW after postcompression. With only 0.19% rms pulse-to-pulse energy fluctuations, the technique exhibits excellent stability. Furthermore, we have measured state-of-the-art spectral-spatial homogeneity and good beam quality of $M^2 = 1.2$ up to a spectral broadening factor of 30. Due to the method's simplicity, compactness, and scalability, it is highly attractive for turning a picosecond laser into an ultrafast light source that generates pulses of only a few tens of femtoseconds duration.

1. Introduction

Femtosecond light pulses are used for a variety of applications including time-resolved fundamental science, material processing, and medical applications [1]. The present ultrafast laser developments reach for increasing peak and average powers [2] in order to advance applications in these fields, for instance by laser-particle acceleration [3], nonlinear attosecond science [4], and raw-event detection utilized in coincidence spectroscopy [5]. Today's most common high-power ultrafast light sources rely on active Yb-ions. A major downside of these lasers is the inability to directly deliver sub-100 fs pulses. Therefore, a multitude of applications requiring shorter pulses cannot readily be addressed. To overcome this limitation, spectral broadening and subsequent pulse compression have become a thriving research topic [6]. Different spectral broadening methods are commonly employed. Due to their excellent power-handling capabilities, bulk nonlinear media and multipass cells (MPCs) employing bulk- or gas-based nonlinear spectral broadening present a vital alternative to fibers or hollow-core capillaries. This was facilitated by the inventions of MPC spectral broadening [7–9] and multiplate continuum generation [10]. In both approaches, the introduced quasi-waveguide results in much better spatial homogeneities of the broadband spectra than in bare bulk experiments which were earlier proposed as a simple method for extending optical pulse bandwidths [11].

Here, we present the combination of both techniques in a single, compact spectral broadening stage. We demonstrate unprecedented high-pulse compression factors of more than 30 (see Figure 1), corresponding to a reduction of the FWHM pulse duration from 1240 fs to 39 fs. Despite strong self-phase modulation, we efficiently suppress spatial

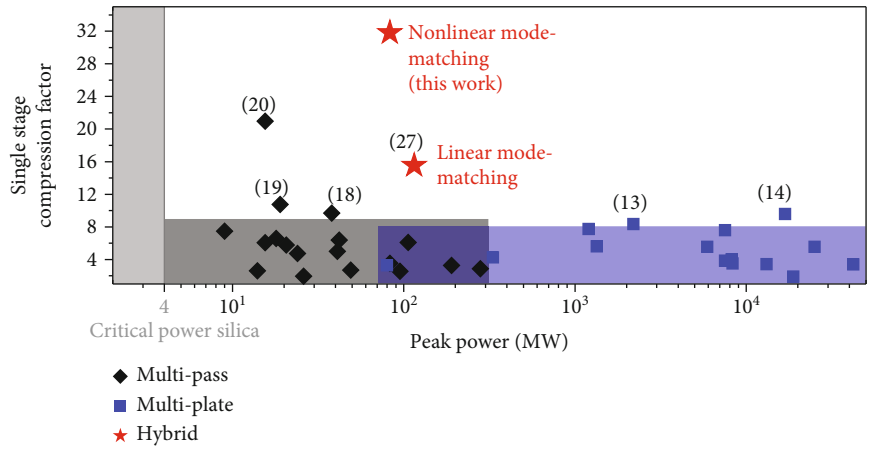

Figure 1: Overview of single-stage compression factors achieved by bulk-based MPCs and the multiplate continuum technique. The dark gray and blue shaded areas enclose the typical operation regimes of the respective compression techniques. References to the experiments with the highest reported single-stage compression factors are provided.

spectrum variations that result from single-pass bulk spectral broadening in the critical self-focusing regime [12]. For comparison, the highest pulse compression factors reported from single multiplate continuum stages are 8.3 [13] and 9.6 [14]. Large compression factors have been achieved with gas-filled MPCs at multi-mJ pulse energy levels [15–17], but only a few single bulk MPC stages were reported to be able to achieve more than 10-fold compression. Those methods, however, either relied on custom-made dispersive mirrors [18] or multi-ps long input pulses being insensitive to dispersion [19, 20]. In contrast, the implementation of our method requires only off-the-shelf optics and enables strong spectral broadening by high B-integrals per pass. Therefore, our compression scheme is a compact alternative to more complex multistage setups [14, 21–25] and presents a highly attractive method to generate sub-50 fs pulses from a high-power picosecond laser.

2. Materials and Methods

2.1. Experimental Design. We compressed the output of a multistage Yb:YAG amplifier operating in 10 Hz burst mode being matched to the pulse trains of the free-electron laser FLASH at DESY [26, 27]. The system delivered pulses centered at 1030 nm wavelength with 112 μJ energy, near Fourier-transform limited 1240 fs pulse duration and a peak power of about 80 MW. Frequency resolved optical gating (FROG) measurements of the pulses are provided in supplement S4. The maximal in-burst average power with minimized pulse-to-pulse energy fluctuations was 112 W. The corresponding 1 MHz pulse repetition rate could be maintained over the burst duration of 800 μs. Typical laser burst shapes are shown in ref. [27]. To avoid saturation of our measurement devices, we used an acousto-optic modulator to adjust the number of pulses in the bursts and their amplitude [27]. Unless stated explicitly, we kept the number of pulses per burst smaller than 50 to circumvent the influence of transient thermal lensing in the main amplifier [27] on our measurement data. The time-dependent thermal effects result in varying beam sizes and divergences within a laser burst. This is different from more common continuous mode lasers which induce constant thermal lenses for the whole pulse train in steady state.

Whereas a high-pressure gas-filled multipass cell could have been used at our peak power level [28], we decided to spectrally broaden the pulses in a bulk-based MPC. This obviated the need for a complex overpressure system. The setup is described in the caption of Figure 2. The employed multilayer MPC mirrors were standard quarter-wave stacks with 200 mm radius of curvature and 50.8 mm diameter. All Kerr media used were stock items. In this way, the setup was kept as simple as possible. We used two focusing lenses and a translation stage for adjusting mode-matching while monitoring the beam size in the targeted focal plane inside the MPC. Herriott-type MPCs exhibit transverse eigenmodes. The input beam is typically matched to the fundamental mode of the Herriott-cell [9] to minimize pass-to-pass beam size oscillations and prevent optical damage.

We measured pulse durations by second-harmonic FROG with a commercial device (Mesa Photonics). In the diagnostics section of the setup, we used a compact grating spectrometer or an optical spectrum analyzer (OSA) for spectrum measurements and a Spiricon M200 M^2-meter for beam quality evaluation. An ANDOR Kymera 193 Czerny-Turner-type spectrograph with a 10 μm horizontal entrance slit and a grating in the $2f$ plane with 500 lines/mm was used for measuring spectral-spatial homogeneity. We placed a FLIR grasshopper CCD camera in the $4f$ -plane that recorded the dispersed spectrum along the horizontal axis and a line-out of the beam along the vertical axis. The wavelength axis was calibrated by comparison to a spectrum recorded with the compact grating spectrometer. The spectral response of the spectrograph was not determined. The beam profiles were measured with the same camera, which had 3.69 μm × 3.69 μm pixel size.

2.2. Simulations. We support our experimental data by nonlinear beam propagation simulations. We employed the

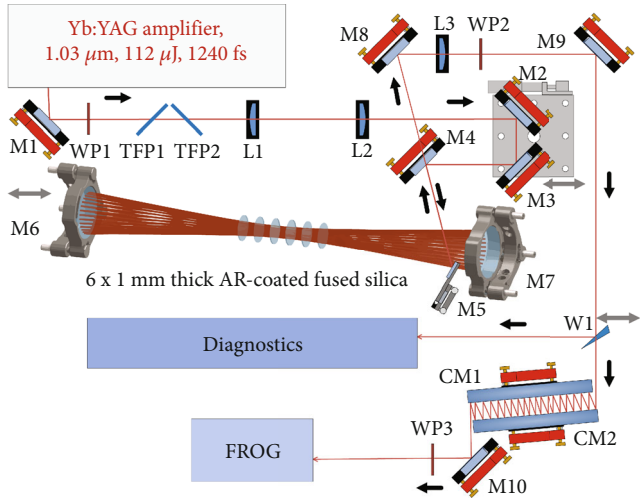

FIGURE 2: Spectral broadening setup. Waveplate WP1 and thin-film polarizers TFP1 and TFP2 are used for polarization cleaning of the Yb:YAG amplifier output. Mode-matching is adjusted with the lenses L1 and L2 as well as the translation stage with mirrors M2 and M3 on it. The mirror M4 is lower than the other mirrors, such that the ingoing beam hits M4 on the top and the outgoing beam is passing it. The focal length of both MPC mirrors M6 and M7 is 100 mm. Pick-off mirror M5 has only a 4 mm vertical aperture to not clip the beam despite of the 32 roundtrips. The six 1 mm thin Kerr media are centered in the about 385 mm long MPC, mounted in lens tubes and spaced by 16 mm. The lens L3 is used for collimation, the waveplate WP2 for readjusting p-polarization to match the specification of the chirped mirrors CM1 and CM2. A wedge is used for sending the beam to all diagnostics except from a FROG-device which is behind the compressor.

SISYFOS code [29] which was previously used for bulk spectral broadening simulations [12]. The Herriott-cell shown in Figure 2 was modeled under the following approximations: the beam was always on the optical axis of the system, the input beam was a fundamental Gaussian ($M^2 = 1$), reflectivity and dispersion of the MPC mirrors as well as transmission of the antireflective (AR) coatings were taken from theoretical data provided by the suppliers. We included the Kerr nonlinearity of air but we neglected the noninstantaneous Raman contributions to the nonlinearities of fused silica and air. Self-steeping was implicitly considered by solving the wave equation in the frequency domain.

Test simulations with both transverse dimensions and a single transverse dimension, exploiting cylindrical symmetry, led to the same outcome. Therefore, we used the computationally less expensive reduced spatial dimensionality with 512 radial grid points. The time and frequency grid, respectively, consisted of 2048 points to properly model the narrow initial and the broad final spectrum.

The Kerr media's nonlinear refractive index, $n_2^{\mathrm{sim}} = 2.5 \cdot 10^{-16}\,\mathrm{cm}^2/\mathrm{W}$, used in simulations was deduced from a comparison between simulation and an MPC experiment with factor ten spectral broadening. It is in good agreement with literature values [30]. We define the spectral broadening factor as the ratio between initial and broadened spectrum transform-limited FWHM pulse durations.

3. Results

3.1. Hybrid Multipass Multiplate Approach. We conducted initial experiments with single silica plates of 3 mm to 10 mm thickness inside an approximately 350 mm long MPC. The thick Kerr media exhibited two drawbacks: First, in addition to spectral broadening, we observed an accumulation of spectral power near the fundamental wavelength of 1030 nm with increasing input pulse energy, indicating a power-dependent mode-mismatch. We even damaged the Kerr medium after extending the MPC to 380 mm length. Second, we measured the spectral phase of pulses compressed by approximately a factor of ten and retrieved a characteristic phase kink near the fundamental wavelength which is known from bulk spectral broadening [12]. We attribute these observations to nonlinear beam reshaping inside the Kerr medium. This is supported by a set of free beam nonlinear propagation simulations that yield a spectral broadening factor of 1.3. The simulations are described in supplement S1. We found that an intense beam propagating through a short medium undergoes significantly less deformation compared to a less intense beam propagating through a longer medium. This indicates that limiting the B-integral per pass, as proposed in the original MPC spectral broadening patent [31], may not be necessary to suppress nonlinear space-time coupling. The B-integral per Kerr medium in multiplate continuum generation was clearly higher than in bulk MPC experiments. Nonetheless, good spatial-spectral homogeneity was reported [14, 32]. Consequently, we used this approach and distributed the nonlinear phase accumulation among a sequence of multiple thin plates inside the Herriott-cell.

Furthermore, Kerr lensing plays a crucial role in multiplate continuum generation because it establishes a quasi-waveguide [12, 32]. We also included the self-focusing effect in the mode-matching calculations (see supplement S2) of our hybrid multipass multiplate scheme. We refer to this as nonlinear mode-matching in bulk MPCs in contrast to linear mode-matching which only considers diffraction. The Herriott cell length is in both cases determined by the mirrors' radii of curvature, the re-entrant condition and the number of passes through the cell [9, 33] but including the Kerr effect yields smaller spot sizes at the mirrors and larger ones in the cell center (see Figure S1). Most importantly, it significantly reduces the pass-to-pass intensity variations in the Kerr media.

Figure 3(a) shows the simulated peak irradiances inside the MPC described in section 2.1. The difference between setting the input beam parameters by linear and nonlinear mode-matching is striking. Whereas for linear mode-matching the peak irradiance in the Kerr media reaches up to $2\,\mathrm{TW/cm}^2$, which would cause coating damage in an experiment, the peak irradiance stays below $500\,\mathrm{GW/cm}^2$ for nonlinear mode-matching, preventing self-focusing induced damage. Consequently, high peak intensities in the nonlinear media can be obtained over all passes by

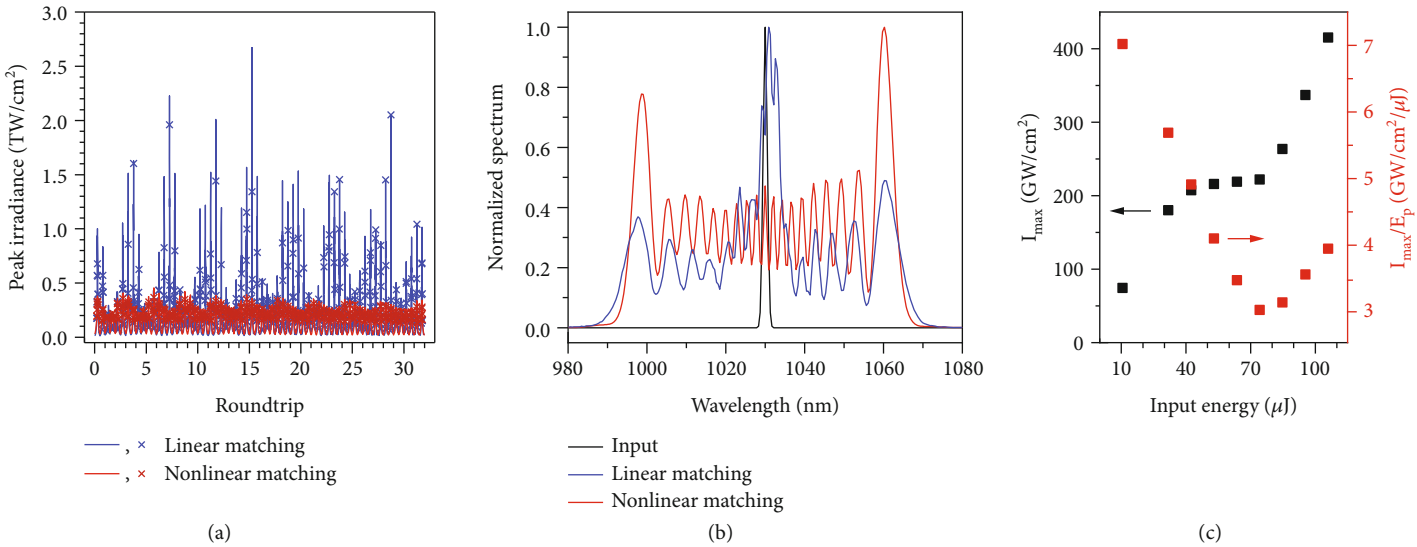

FIGURE 3: (a) Comparison of simulated peak irradiances inside the MPC shown in Figure 2(a) for 100 μJ, 1250 fs Gaussian input pulses in case of linear (blue line) and nonlinear (red line) mode-matching. The crosses indicate the locations of the silica plates. Nonlinear mode-matching significantly reduces the maximal peak irradiance. Residual peak irradiance oscillations are caused by the approximations of our analytical model presented in supplement S2. Best mode-matching, i.e., smallest pass-to-pass beam area variation, is accomplished for 75 μJ input pulses according to (c). (b) Output spectra after 32 roundtrips corresponding to irradiance evolution from (a) and comparison to the input spectrum. (c) Simulated dependence of maximal peak irradiance in the Kerr media (I_{max}) on input pulse energy (E_p) for a nonlinear mode-matching point of about 75 μJ where I_{max}/E_p reaches its minimum. The monotonic increase of I_{max} obviates the need for modifying the input beam during energy ramp-up in a nonlinear mode-matching setting.

accounting for Kerr lensing. This, in turn, enables higher spectral broadening factors from a single stage. A recent theory paper has also pointed out the importance of nonlinear mode-matching in gas-filled MPCs that operate in the subcritical self-focusing regime [34]. The irradiance enhancement predicted for the bulk MPC studied here is, however, more than 10 times higher than in the numerical example of ref. [34].

The simulated shapes of the nonlinearly broadened spectra indicate the quality of mode-matching (see Figure 3(b)). With nonlinear mode-matching, the outermost spectral lobes exhibit the highest spectral power. This qualitatively corresponds to textbook examples of self-phase modulated spectra in fiber schemes [35]. By contrast, excessive spectral power is concentrated near the fundamental wavelength if the input beam is matched to the Kerr-lensing free Herriott-cell mode (blue solid line). This is in agreement with our experimental observations. For a large mode-mismatch, the Kerr-effect induces the excitation of higher-order modes. These overlap only partially with the intense main beam in the Kerr media [12] and lead to the emergence of the unbroadened feature in the spectrum. We note that a distinct peak around 1030 nm is also caused by input pulse pedestals or pre/post pulses which are not intense enough for significant self-phase modulation. This peak is, however, independent of power launched into the MPC.

3.2. Spectral Broadening and Pulse Compression Experiments. In order to verify the occurrence of self-focusing and to determine an experimental nonlinear refractive index, we conducted Z-scan-type measurements inside the MPC (see supplement S3). We used the result to calculate the beam parameters for nonlinear mode-matching and aligned the MPC correspondingly (see supplement S2 for details). We did not adjust any optics while increasing the input power but expected the laser beam to be matched to the Herriott-cell at full input energy. This is possible because the maximal peak irradiances in the Kerr media monotonically increase with input pulse energy according to our simulations shown in Figure 3(c).

Figure 4(a) shows a set of measured broadened spectra that were recorded behind the MPC while the laser pulse energy was increased. The derived dependence of the spectral broadening factor on the measured output pulse energy is plotted in Figure 4(b). The dispersion of the six Kerr plates yielded saturation of self-phase modulation at high input powers. The broadened spectra supported sub-40 fs pulses for output energies of at least 75 μJ. The highest achieved spectral broadening factor was 33, corresponding to a reduction of bandwidth-limited pulse duration from 1.2 ps to 36 fs. The measured spectra in Figure 4(a) exhibit a central spectral peak which can be clearly distinguished from the self-phase modulated parts of the spectra at 16 μJ or higher output energies. Its independence of output power implies that it was caused by the pedestal of the input pulses, which we measured by FROG (see supplement S4), and not by a strong mode-mismatch. Aside from that, the spectral shape agrees well with the simulated one in Figure 3(b) up to approximately 50 μJ output energy. For higher energies, the spectral modulations flatten out at parts of the spectrum and the symmetry with respect to the fundamental wavelength decreases. We attribute this to the spurious four-wave mixing which was qualitatively predicted in simulations (see supplement S5) and was experimentally confirmed

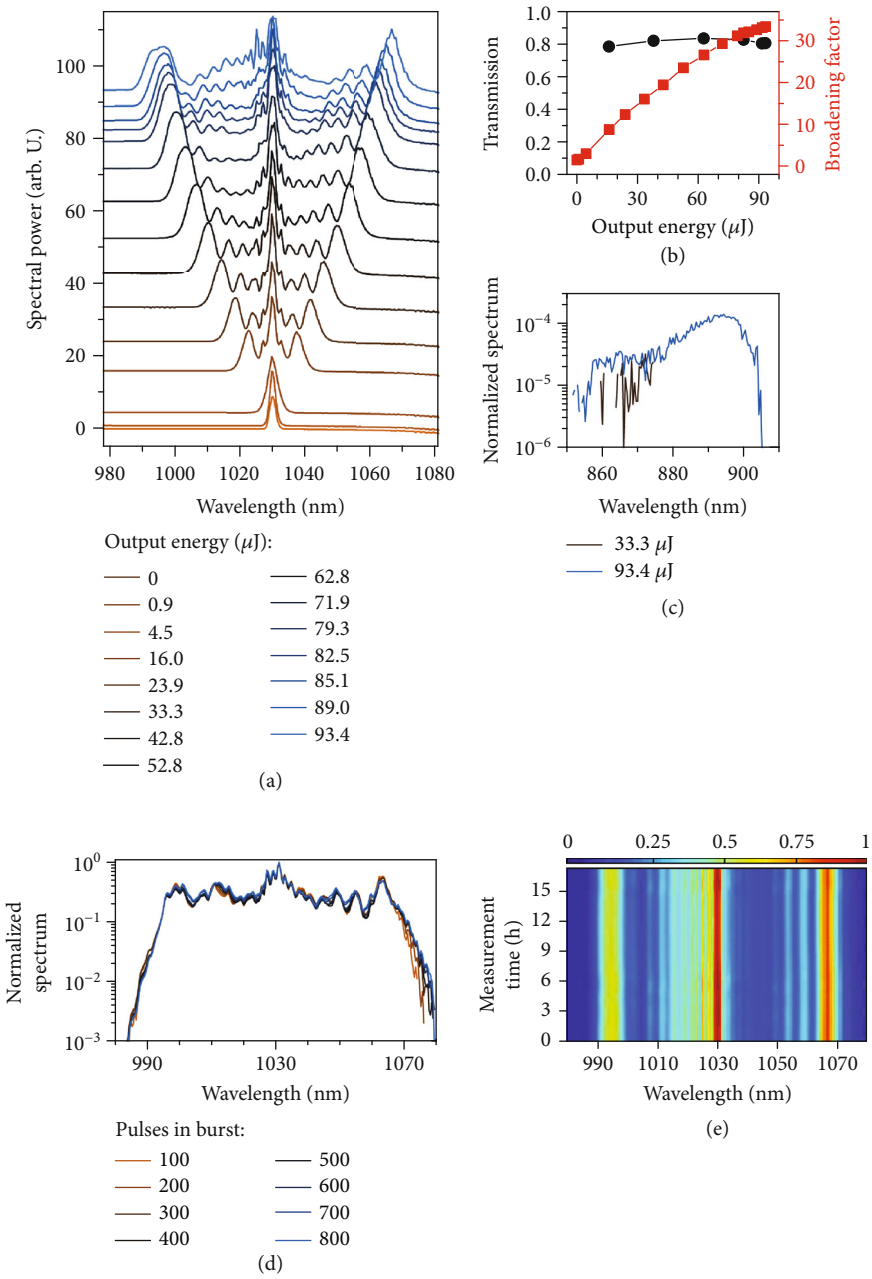

Figure 4: (a) Broadened spectra after 32 roundtrips in a 385 mm long MPC detected with a response function corrected grating spectrometer. The spectra are offset by the output energy measured with an energy meter and corrected by the wedge W1 transmission. 0 μJ refers to the input spectrum. (b) Corresponding spectral broadening factors as a function of output pulse energy. The transform-limited pulse duration at full power is more than 30 times shorter than at the input. The MPC transmission is constantly about 80%. (c) Spectral side-bands, becoming detectable for more than 30 μJ output energy. These are excited by four-wave mixing as qualitatively predicted by simulations. The spectra are normalized to the maximum of the respective self-phase modulated part near 1030 nm. (d) Spectral broadening in dependence of pulses per burst. Despite the strongly changing beam parameters caused by transient thermal lenses in the main amplifier, the large broadening factor is preserved. (e) Spectrum stability measured over 17 hours with one recording per second.

as shown in Figure 4(c). The generation of spectral side-bands was previously observed in gas-filled MPC experiments [15, 36] and was studied explicitly in a simulation paper [37]. First signatures could be detected approximately 50 dB below the maximal power spectral density for 30 μJ output pulse energy. At maximum power, the amplitude of this short wavelength feature becomes one order of magnitude stronger. We note that the mixed frequencies lie outside of the reflection band of our dielectric optics, and thus the measured spectrum does not represent the magnitude and central frequency of the side-bands generated inside the MPC. Our simulation also predicts spectral components

around 1125 nm (see Figure S5(b)) which are outside of our detection range and could not be observed.

We note that the Fourier transform-limit was independent of the number of pulses per laser burst, i.e. the same spectral broadening characteristics were also obtained with 112 W average power over the maximal 800 μs burst duration (see Figure 4(d)). This demonstrates the robustness of the MPC approach. Owing to strong nonstationary thermal lenses in the Yb:YAG amplifier, beam divergence and size change significantly over the 800 μs burst duration [27]. This would cause severe output power modulations in fiber spectral broadening schemes that only transmit modes matched to the waveguide. Despite the large spectral broadening factor, the measured spectrum was highly stable as Figure 4(e) demonstrates. From one recording per second in an overnight measurement (≈17 hours measurement time), we computed a standard deviation of the Fourier-transform limited pulse duration of only 0.1 fs at 35.7 fs mean value. The pulse-to-pulse energy fluctuations after the MPC exhibited only a 0.19% standard deviation relative to the mean output energy. The measurements were performed with a single pulse per burst. Spectrum and pulse energy were logged in parallel.

To shorten the spectrally broadened pulses, we set-up a chirped-mirror compressor inducing a group delay dispersion (GDD) of -200 fs^2 per reflection. For best compression, we changed the number of bounces in steps of four and slightly varied the input pulse energy to the MPC. By means of second harmonic FROG, we could at best retrieve a FWHM duration of 39 fs (Figure 5), corresponding to a factor 32 pulse duration shortening in comparison to the 1.24 ps input shown in supplement S4. Considering the pedestals of the input pulses, the deduced 70% energy content in the main peak is close to the theoretical limit of compressing a self-phase modulated Gaussian by compensating linear chirp [38]. The required 72 bounces off the chirped mirrors applied a total GDD of -14,400 fs^2 to the pulses and resulted in only 78% transmission of the compressor. Moreover, we measured 5% depolarization after waveplate WP2 by inserting a polarizing beamsplitting cube into the uncompressed beam. As the losses are small, we did not try to reduce them further by a quarter-wave plate. The depolarization is caused by the large nonlinear phase shift in the MPC which effectively amplifies residual cross-polarized light. Intrapulse depolarization is also known from fiber spectral broadening [39]. The usable pulse energy after compression accumulated to 65 μJ which yielded a peak power of 1.1 GW. By contrast to other bulk-MPC or multiplate experiments [21, 22, 40], we did not observe a phase kink near the fundamental wavelength (Figure 5(a)).

3.3. Beam Characterization. Figure 6(a) shows a camera image after the 4f spectrograph at full spectral broadening. The frequency content is nearly uniformly distributed across the beam axis. We calculated a mean spectral homogeneity along the vertical beam axis of $\bar{V}_y = 97.3\%$, following the figure of merit proposed by Weitenberg et al. [41] (see supplement S6). A homogeneity of $\bar{V}_y = 97.3\%$ was also measured for a gas-filled MPC with comparable spectral broadening from 1.3 ps to 39 fs bandwidth limit [15]. This underscores that the detrimental spatial effects, which are typical for single-pass spectral broadening in the critical self-focusing regime, have been largely suppressed by the multipass multiplate approach.

Although the near- and far-field beam profiles for the highest spectral broadening factor displayed in Figure 6(b) look close to Gaussian, we determined a distinct increase of the M^2 parameters to 1.6×1.5 at full input power. Figure 6(c) shows that we measured M^2 values of about 1.2 for all input energies up to 90 μJ, corresponding to a spectral broadening factor of about 30. However, for higher input energies, a gradual decrease of beam quality was recorded. A similar observation was reported in the first MPC paper by Schulte et al. [7] and attributed to thermal effects. In our work, we could run experiments at only 10 Hz pulse repetition rate and can thus exclude thermal effects. In ref. [42], the degradation was interpreted as an onset of bulk-like broadening. This is, however, in contradiction to our compression and spectral homogeneity measurements. An experiment with the same input energy but considerably less roundtrips (blue markers Figure 6(c)) suggests that the higher M^2 values are caused by parasitic nonlinear effects in the MPC. We suspect that the four-wave mixing process (see S4, Figure 4(c)) between broadened spectrum and unbroadened mode-mismatched pulse pedestal introduced nonperiodic losses in the MPC which led to reshaping of the beam. Therefore, input pulse shaping could further improve the output beam quality.

4. Discussion

We have presented a hybrid bulk multipass multiplate method for spectral broadening of ultrashort laser pulses. This novel approach yielded significantly higher single-stage compression factors than previously reported from the individual techniques. In total, the laser beam passed 384 Kerr media in our setup. On the one hand, this is practically impossible to implement in a pure multiplate scheme where less than ten passes are typical. On the other hand, to our knowledge all bulk-MPC papers roughly followed the initial proposal that the B-integral per pass through the Herriott-cell should not exceed $\pi/5$ [31]. The simulations shown in Figure 3 predict B-integrals per pass of up to $B \approx 4\pi/5$ resulting from an average peak irradiance $<I_p> = 285$ GW/cm^2 inside the six Kerr media. This was achieved through the introduction of multiple thin plates and explains why the presented 32-fold pulse duration reduction has not been accomplished with the bulk-MPC technique alone. It is only comparable to the best results demonstrated with gas-filled MPCs which operate in the subcritical self-focusing regime [15–17]. By contrast to merely increasing the number of roundtrips in the MPC to attain large nonlinear phase shifts, the nonlinear mode-matching technique minimizes peak intensity variations in the Kerr media, and thus enables large spectral broadening factors by high intensities and not primarily by long propagation lengths in the nonlinear

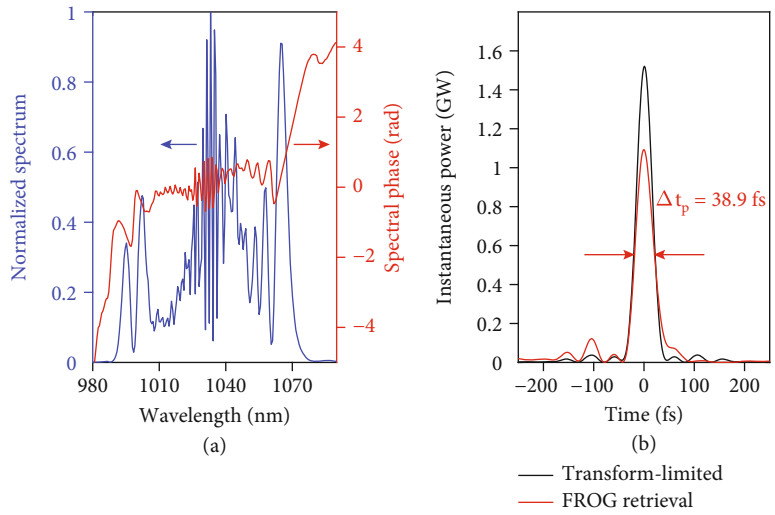

FIGURE 5: (a) Retrieved FROG spectrum and spectral phase of the postcompressed pulses. (b) Retrieved pulse shape with 70.1% of energy within the $2\Delta t_p$ width compared to the transform limited pulse (Δt_p = 35.6 fs, 86.4% of energy within $2\Delta t_p$ width) for 65 μJ pulse energy. Δt_p denotes the FWHM of the pulse intensity.

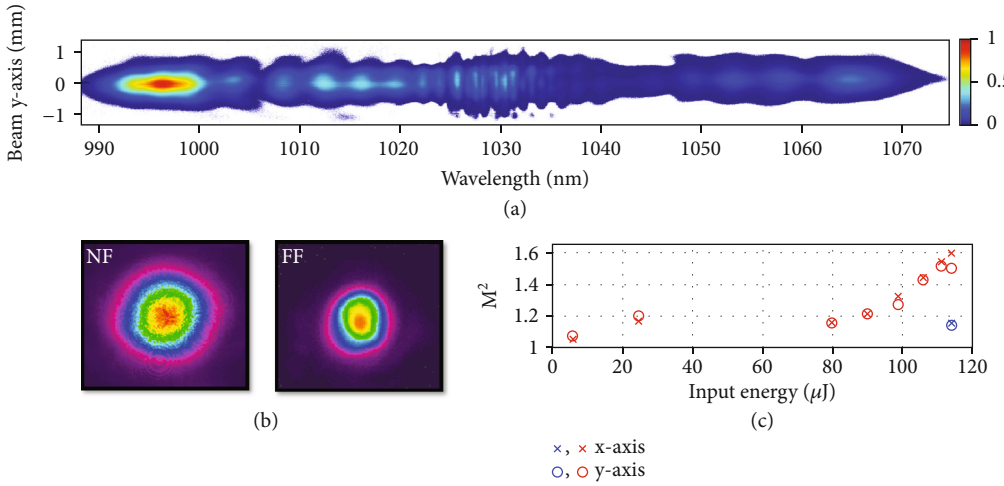

FIGURE 6: (a) Measured spectra across the vertical beam axis for a 36 fs Fourier transform-limit. (b) Near-field (NF) and far-field (FF) profiles, also recorded at 36 fs Fourier transform-limit. (c) Experimentally determined M^2 parameters for 32 roundtrips (red markers) and 8 roundtrips (blue markers).

material. This is essential if dispersion induces pulse stretching, i.e. for generating ultrashort pulses. Despite the large single-pass B-integrals and operating approximately 20 times above the critical power of the nonlinear material, we could vastly suppress undesired features of bulk spectral broadening, such as spectral inhomogeneity across the beam profile and the typical phase kink near the input wavelength. This was enabled by distributing the Kerr nonlinearity along the MPC instead of using one thick fused silica window. The demonstrated approach was implemented with standard quarter-wave stack mirrors and off-the-shelf Kerr media. Neither a vacuum or high-pressure compatible enclosure, nor dispersive MPC mirrors were needed. Moreover, the setup was very compact and excellent stability was demonstrated. This makes the method highly attractive for turning a picosecond laser into an ultrafast light source generating sub-50 fs pulses. Whereas we measured constantly good beam quality up to a spectral broadening factor of 30, the M^2 value increased from 1.2 to 1.6 upon reducing the Fourier-transform limit further from 40 fs to 36 fs. We attribute this to parasitic four-wave mixing in the MPC which, according to our simulations, could be circumvented by pedestal-free input pulses.

The main obstacle for generating even shorter pulses with our approach is the bandwidth of the used optics. The MPC mirrors support durations of about 30 fs. Replacing tantalum pentoxide by titania as high index material of the quarter-wave stack mirrors would enable the generation of about 20 fs pulses. By using enhanced metallic mirrors, even few-cycle pulses were demonstrated [16, 43]. Conventional antireflection coatings would lead to clearly lower MPC transmissions if larger bandwidths with the same number

of roundtrips are targeted. If the typically circular Herriott-pattern is rendered strongly elliptical, such that polarization rotation is negligible, the Kerr-media could be placed at Brewster's angle into the MPC [44]. However, this would cause a higher spot density and enforce less roundtrips than for a circular pattern or larger mirrors. Furthermore, the impact of different lensing in sagittal and tangential planes would have to be investigated. Alternatively, nanotextured surfaces exhibit very low Fresnel reflections over a large spectral range [45]. This opens the perspective of few-cycle pulse generation by the hybrid multipass multiplate approach. Moreover, the Kerr media can be moved closer to the MPC mirrors if laser peak power increases [7], and thus the proposed scheme can be employed in the 5 MW to 5 GW range without the need for Herriott-cells exceeding usual optical table lengths. For certain high peak power applications, bulk-MPCs may present interesting alternatives to gas-filled MPCs. Gas ionization and mirror damage thresholds differ by orders of magnitudes. Therefore, gas-filled MPCs are usually operated near the stability edge. In contrast, bulk Kerr media and dielectric mirrors exhibit comparable damage thresholds. Consequently, very compact Herriott-cells that do not compromise spectral broadening are possible. Bulk spectral broadening is also envisioned for PW class lasers [46]. Similar to high-power multipass amplifier research, where thermal lenses need to be considered, peak power-scaling of the bulk-MPC approach would require to find a compact resonator design that can handle Kerr lensing. A possible solution is the use of folded bow-tie cavities [44].

The applicability of the demonstrated hybrid multipass multiplate scheme to state-of-the-art ultrafast lasers demands its average power scalability. We conducted the spectral broadening experiments with a burst-mode laser delivering average powers of up to 112 W within the 800 μs duty cycle and about 0.9 W over the 100 ms burst period. Thermal effects evolve on the ns to ms time scale depending on thermal material properties and beam sizes [47]. In the used Yb:YAG amplifier, thermal equilibrium is reached after 2 to 3 ms of pumping, that is on the order of the burst duration. The transient thermal lenses in the amplifier lead to strongly changing beam parameters over the burst. Their impact on spectral broadening in an MPC was investigated in more detail in ref. [27]. Although we conducted most of the experiments with a small number of pulses which simplified data analysis, we have demonstrated that the hybrid spectral broadening approach is resistant against these detrimental nonstationary thermal effects, which cannot be accounted for in the mode-matching procedure (see Figure 4(d)). This shows that our approach exhibits a relatively large beam parameter acceptance range, and thus will also tolerate thermal effects inside the MPC depending on the intensities used in the Herriott-cell. In our experiments, we estimated the maximal peak irradiance in the Kerr plates to be only about 25% of the damage threshold we measured. Therefore, small thermal lenses in the MPC will not cause damage to the used optics. We have estimated the thermal nonlinearities in the Kerr media following ref. [47] in supplement S7 and predict that they only become relevant at the 10 kW average power level. This is in good agreement with multiple bulk MPCs which were demonstrated with several hundreds of watts of average power [7, 41] and did not report decisive issues caused by thermal load. We note that in Kerr lens mode-locked thin-disk oscillators kW-level average powers are focused into thin Kerr-media [48, 49]. In an enhancement cavity with up to 160 kW average power, it was shown that the thermal lenses of a thin silica plate and the cavity mirrors can be balanced [50]. These literature examples provide further evidence that the proposed spectral broadening scheme is average power scalable.

In conclusion, the hybrid multipass multiplate approach has enabled record-high single-stage pulse compression factors for these bulk spectral broadening methods. The demonstrated efficiency, beam, and pulse quality are comparable to less compact and more complex multistage setups. In contrast to gas-filled MPCs, no sealed enclosure of the setup is required and our approach can be applied to a large peak power range. Therefore, it is a very attractive method for pulse-compression of state-of-the-art laser systems and opens perspectives for novel high-repetition rate extreme light sources operating in the few-cycle or TW to PW peak power regime.

Data Availability

Data can be obtained from the corresponding author upon reasonable request.

Conflicts of Interest

The authors declare that there is no conflict of interest regarding the publication of this article.

Authors' Contributions

M. Seidel conceived the hybrid spectral broadening scheme, conducted experiments as well as simulations, and led the writing of the manuscript. P. Balla implemented the initial setup and conducted the initial experiments. C. Li and L. Winkelmann aligned the laser used for the experiments. G. Arisholm developed the SISYFOS code and adapted it to MPC simulations. L. Winkelmann, I. Hartl, and C.M. Heyl initiated the project. I. Hartl and C.M. Heyl conceived the initial setup and supervised the project. All authors revised the manuscript and contributed to the writing of it.

Acknowledgments

We thank Caterina Vidoli for proof-reading the initially submitted manuscript and DESY (Hamburg, Germany), a member of the Helmholtz Association HGF, for the provision of experimental facilities.

Supplementary Materials

Supplementary 1. Supplemented sections: Supplement S1 describes the simulations of single-pass irradiance enhancement inside Kerr media of different lengths. The results are shown in Table S1. Supplement S2 describes the ABCD

matrix calculus for nonlinear mode-matching. Fig. S1 visualizes the calculation results. Supplement S3 describes the performed Z-scan measurements. Fig. S2 shows the Z-scan setup and the measurement results. Supplement S4 describes FROG measurements of the input pulses and provides supplementary information to the FROG measurements of the postcompressed pulses. Fig. S3 shows the input pulse FROG measurement results and Fig. S4 the FROG traces of the postcompressed pulses as well as the corresponding spectra. Supplement S5 discusses the parasitic four-wave mixing effect which is observed in the experimental data. Corresponding simulation results are provided in Fig. S5. Supplement S6 provides the equations used for homogeneity calculations. Supplement S7 estimates the thermal lenses in the Kerr media. The supplementary materials contain the additional references [51–55].

Supplementary 2. Supplemented animation: the supplemented gif-file shows a sequence of line-outs of Fig. S5c–d.

References

[1] G. Mourou, "Nobel Lecture: Extreme light physics and application," *Reviews of Modern Physics*, vol. 91, no. 3, article 030501, 2019.

[2] H. Fattahi, H. G. Barros, M. Gorjan et al., "Third-generation femtosecond technology," *Optica*, vol. 1, no. 1, p. 45, 2014.

[3] F. Albert, M. E. Couprie, A. Debus et al., "2020 roadmap on plasma accelerators," *New Journal of Physics*, vol. 23, no. 3, article 031101, 2021.

[4] I. Orfanos, I. Makos, I. Liontos et al., "Attosecond pulse metrology," *APL Photonics*, vol. 4, no. 8, article 080901, 2019.

[5] S. Mikaelsson, J. Vogelsang, C. Guo et al., "A high-repetition rate attosecond light source for time-resolved coincidence spectroscopy," *Nanophotonics*, vol. 10, no. 1, pp. 117–128, 2020.

[6] T. Nagy, P. Simon, and L. Veisz, "High-energy few-cycle pulses: Post-compression techniques," *Advances in Physics: X*, vol. 6, no. 1, article 1845795, 2021.

[7] J. Schulte, T. Sartorius, J. Weitenberg, A. Vernaleken, and P. Russbueldt, "Nonlinear pulse compression in a multi-pass cell," *Optics Letters*, vol. 41, no. 19, pp. 4511–4514, 2016.

[8] M. Hanna, F. Guichard, N. Daher, Q. Bournet, X. Delen, and P. Georges, "Nonlinear Optics in Multipass Cells," *Laser & Photonics Reviews*, vol. 15, no. 12, article 2100220, 2021.

[9] A.-L. Viotti, M. Seidel, E. Escoto et al., "Multi-Pass Cells for Post-Compression of Ultrashort Laser Pulses," *Optica*, vol. 9, no. 2, pp. 197–216, 2022.

[10] C.-H. Lu, Y.-J. Tsou, H.-Y. Chen et al., "Generation of intense supercontinuum in condensed media," *Optica*, vol. 1, no. 6, p. 400, 2014.

[11] C. Rolland and P. B. Corkum, "Compression of high-power optical pulses," *Journal of the Optical Society of America B*, vol. 5, no. 3, p. 641, 1988.

[12] M. Seidel, G. Arisholm, J. Brons, V. Pervak, and O. Pronin, "All solid-state spectral broadening: An average and peak power scalable method for compression of ultrashort pulses," *Optics Express*, vol. 24, no. 9, p. 9412, 2016.

[13] P.-C. Huang, C. Hernandez-Garcia, J.-T. Huang et al., "Polarization control of isolated highharmonic pulses," *Nature Photonics*, vol. 12, no. 6, pp. 349–354, 2018.

[14] C.-H. Lu, W.-H. Wu, S.-H. Kuo et al., "Greater than 50 times compression of 1030 nm Yb:KGW laser pulses to single-cycle duration," *Optics Express*, vol. 27, no. 11, pp. 15638–15648, 2019.

[15] M. Kaumanns, V. Pervak, D. Kormin et al., "Multipass spectral broadening of 18 mJ pulses compressible from 13 ps to 41 fs," *Optics Letters*, vol. 43, no. 23, pp. 5877–5880, 2018.

[16] P. Balla, A. BinWahid, I. Sytcevich et al., "Postcompression of picosecond pulses into the few-cycle regime," *Optics Letters*, vol. 45, no. 9, pp. 2572–2575, 2020.

[17] M. Kaumanns, D. Kormin, T. Nubbemeyer, V. Pervak, and S. Karsch, "Spectral broadening of 112 mJ, 13 ps pulses at 5 kHz in a LG 10 multipass cell with compressibility to 37 fs," *Optics Letters*, vol. 46, no. 5, pp. 929–932, 2021.

[18] S. Gröbmeyer, K. Fritsch, B. Schneider et al., "Self-compression at 1 um wavelength in all-bulk multi-pass geometry," *Applied Physics B*, vol. 126, no. 10, p. 159, 2020.

[19] J. Song, Z. Wang, R. Lv et al., "Generation of 172 fs pulse from a Nd: YVO4 picosecond laser by using multi-pass-cell technique," *Applied Physics B*, vol. 127, no. 4, p. 50, 2021.

[20] J. Song, Z. Wang, X. Wang et al., "Generation of 601 fs pulse from an 8 kHz Nd:YVO4 picosecond laser by multi-pass-cell spectral broadening," *Chinese Optics Letters*, vol. 19, no. 9, article 093201, 2021.

[21] K. Fritsch, M. Poetzlberger, V. Pervak, J. Brons, and O. Pronin, "All-solid-state multipass spectral broadening to sub-20 fs," *Optics Letters*, vol. 43, no. 19, pp. 4643–4646, 2018.

[22] E. Vicentini, Y. Wang, D. Gatti et al., "Nonlinear pulse compression to 22 fs at 156 μJ by an all-solid-state multipass approach," *Optics Express*, vol. 28, no. 4, pp. 4541–4549, 2020.

[23] G. Barbiero, H. Wang, J. Brons, B.-H. Chen, V. Pervak, and H. Fattahi, "Broadband terahertz solid-state emitter driven by Yb:YAG thin-disk oscillator," *Journal of Physics B: Atomic, Molecular and Optical Physics*, vol. 53, no. 12, article 125601, 2020.

[24] C.-L. Tsai, F. Meyer, A. Omar et al., "Efficient nonlinear compression of a mode-locked thin-disk oscillator to 27 fs at 98 W average power," *Optics Letters*, vol. 44, no. 17, pp. 4115–4118, 2019.

[25] G. Barbiero, H. Wang, M. Gral et al., "Efficient nonlinear compression of a thin-disk oscillator to 8.5 fs at 55 W average power," *Optics Letters*, vol. 46, no. 21, pp. 5304–5307, 2021.

[26] C. Li, L. Winkelmann, and I. Hartl, "Flexible Pulse-Shape Picosecond Front-End for XFEL Photocathode Lasers," in *Conference on Lasers and Electro-Optics*, San Jose, California: OSA, 2019.

[27] M. Seidel, F. Pressacco, O. Akcaalan et al., "Ultrafast MHz-rate burst-mode pump-probe laser for the FLASH FEL facility based on nonlinear compression of ps-level pulses from an Yb-amplifier chain," *Laser & Photonics Reviews*, vol. 16, article 2100268, 2022.

[28] L. Lavenu, M. Natile, F. Guichard et al., "Highpower two-cycle ultrafast source based on hybrid nonlinear compression," *Optics Express*, vol. 27, no. 3, pp. 1958–1967, 2019.

[29] G. Arisholm and H. Fonnum, *Simulation System For Optical Science (SISYFOS) tutorial, version 2*, Norwegian Defence Research Establishment (FFI), 2021.

[30] D. Milam, "Review and assessment of measured values of the nonlinear refractive-index coefficient of fused silica," *Applied Optics*, vol. 37, no. 3, pp. 546–550, 1998.

[31] A. Vernaleken, P. Rubuldt, T. Sartorius, J. Schulte, and J. Weitenberg, "Method and arrangement for the spectral broadening of laser pulses for non-linear pulse compression," US Patent 9,847,615, 2017.

[32] Y.-C. Cheng, C.-H. Lu, Y.-Y. Lin, and A. H. Kung, "Supercontinuum generation in a multiplate medium," *Optics Express*, vol. 24, no. 7, pp. 7224–7231, 2016.

[33] D. Herriott, H. Kogelnik, and R. Kompfner, "Off-Axis Paths in Spherical Mirror Interferometers," *Applied Optics*, vol. 3, no. 4, pp. 523–526, 1964.

[34] M. Hanna, L. Daniault, F. Guichard et al., "Nonlinear beam matching to gas-filled multipass cells," *OSA Continuum*, vol. 4, no. 2, pp. 732–738, 2021.

[35] G. Agrawal, "Self-Phase Modulation," in *Nonlinear Fiber Optics*, Elsevier, 2013.

[36] P. Russbueldt, J. Weitenberg, J. Schulte et al., "Scalable 30 fs laser source with 530 W average power," *Optics Letters*, vol. 44, no. 21, pp. 5222–5225, 2019.

[37] M. Hanna, N. Daher, F. Guichard, X. Delen, and P. Georges, "Hybrid pulse propagation model and quasi-phase-matched four-wave mixing in multipass cells," *Journal of the Optical Society of America B*, vol. 37, no. 10, pp. 2982–2988, 2020.

[38] A.-L. Viotti, S. Alisauskas, H. Tunnermann et al., "Temporal pulse quality of a Yb:YAG burst-mode laser post-compressed in a multi-pass cell," *Optics Letters*, vol. 46, no. 18, pp. 4686–4689, 2021.

[39] G. Agrawal, "Polarization effects, cross-phase modulation," in *Nonlinear Fiber Optics*, Elsevier, 2013.

[40] C.-L. Tsai, Y.-H. Tseng, A.-Y. Liang, M.-W. Lin, S.-D. Yang, and M.-C. Chen, "Nonlinear Compression of Intense Optical Pulses at 1.55 μm by Multiple Plate Continuum Generation," *Journal of Lightwave Technology*, vol. 37, no. 19, pp. 5100–5107, 2019.

[41] J. Weitenberg, A. Vernaleken, J. Schulte et al., "Multi-pass-cell-based nonlinear pulse compression to 115 fs at 75 μJ pulse energy and 300 W average power," *Optics Express*, vol. 25, no. 17, pp. 20502–20510, 2017.

[42] M. Hanna, X. Delen, L. Lavenu et al., "Nonlinear temporal compression in multipass cells: Theory," *Journal of the Optical Society of America B*, vol. 34, no. 7, p. 1340, 2017.

[43] M. Müller, J. Buldt, H. Stark, C. Grebing, and J. Limpert, "Multipass cell for high-power few-cycle compression," *Optics Letters*, vol. 46, no. 11, p. 2678, 2021.

[44] C. M. Heyl, M. Seidel, E. Escoto et al., "High-energy bow tie multi-pass cells for nonlinear spectral broadening applications," *Journal of Physics: Photonics*, vol. 4, no. 1, 2022.

[45] D. S. Hobbs, B. D. MacLeod, and E. S. III, "Continued advancement of laser damage resistant optically functional microstructures," in *Laser-induced damage in optical materials: 2012*, G. J. Exarhos, V. E. Gruzdev, J. A. Menapace, D. Ristau, and M. J. Soileau, Eds., vol. 8530, SPIE, 2012.

[46] E. A. Khazanov, S. Y. Mironov, and G. A. Mourou, "Nonlinear compression of high-power laser pulses: Compression after compressor approach," *Physics-Uspekhi*, vol. 62, no. 11, pp. 1096–1124, 2019.

[47] R. W. Boyd, "Chapter 4 - The Intensity-Dependent Refractive Index," in *Nonlinear Optics (Third Edition)*, R. W. Boyd, Ed., pp. 207–252, Academic Press, Burlington, 2008.

[48] J. Brons, V. Pervak, E. Fedulova et al., "Energy scaling of Kerr-lens mode-locked thin-disk oscillators," *Optics Letters*, vol. 39, no. 22, p. 6442, 2014.

[49] J. Fischer, J. Drs, N. Modsching, F. Labaye, V. J. Wittwer, and T. Südmeyer, "Efficient 100- MW, 100-W, 50-fs-class Yb:YAG thin-disk laser oscillator," *Optics Express*, vol. 29, no. 25, article 42075, 2021.

[50] N. Lilienfein, H. Carstens, S. Holzberger et al., "Balancing of thermal lenses in enhancement cavities with transmissive elements," *Optics Letters*, vol. 40, no. 5, p. 843, 2015.

[51] A. Sennaroglu and J. Fujimoto, "Design criteria for Herriott-type multi-pass cavities for ultrashort pulse lasers," *Optics Express*, vol. 11, no. 9, p. 1106, 2003.

[52] D. R. Herriott and H. J. Schulte, "Folded Optical Delay Lines," *Applied Optics*, vol. 4, no. 8, p. 883, 1965.

[53] A. E. Siegman, *Lasers, Revised*, University Science Books, Sausalito, California, 1986.

[54] L. Yan, Y.-Q. Liu, and C. Lee, "Pulse temporal and spatial chirping by a bulk Kerr medium in a regenerative amplifier," *IEEE Journal of Quantum Electronics*, vol. 30, no. 9, pp. 2194–2202, 1994.

[55] "Heraeus Transmission Calculator for Optical Applications," 2022, http://www.heraeus.com/en/hca/fused_silica_quartz_knowledge_base_1/t_calc_1/transmission_calc_opt/transmission_calculator_opt.html.